ARTICLE

Biodegradable Fibrous Scaffolds with Tunable Properties Formed from Photo-Cross-Linkable Poly(glycerol sebacate)

Jamie L. Ifkovits,[†] Jeffrey J. Devlin,[†] George Eng,[‡] Timothy P. Martens,[‡] Gordana Vunjak-Novakovic,[‡] and Jason A. Burdick*,[†]

Department of Bioengineering, University of Pennsylvania, Philadelphia, Pennsylvania 19104, and Department of Biomedical Engineering, Columbia University, New York, New York 10032

ABSTRACT It is becoming increasingly apparent that the architecture and mechanical properties of scaffolds, particularly with respect to mimicking features of natural tissues, are important for tissue engineering applications. Acrylated poly(glycerol sebacate) (Acr-PGS) is a material that can be cross-linked upon exposure to ultraviolet light, leading to networks with tunable mechanical and degradation properties through simple changes during Acr-PGS synthesis. For example, the number of acrylate functional groups on the macromer dictates the concentration of cross-links formed in the resulting network. Three macromers were synthesized that form networks that vary dramatically with respect to their tensile modulus (~30 kPa to 6.6 MPa) and degradation behavior (~20−100% mass loss at 12 weeks) based on the extent of acrylation (~1−24%). These macromers were processed into biodegradable fibrous scaffolds using electrospinning, with gelatin as a carrier polymer to facilitate fiber formation and cell adhesion. The resulting scaffolds were also diverse with respect to their mechanics (tensile modulus ranging from ~60 kPa to 1 MPa) and degradation (~45−70% mass loss by 12 weeks). Mesenchymal stem cell adhesion and proliferation on all fibrous scaffolds was indistinguishable from those of controls. The scaffolds showed similar diversity when implanted on the surface of hearts in a rat model of acute myocardial infarction and demonstrated a dependence on the scaffold thickness and chemistry in the host response. In summary, these diverse scaffolds with tailorable chemical, structural, mechanical, and degradation properties are potentially useful for the engineering of a wide range of soft tissues.

KEYWORDS: electrospinning • elastomer • tissue engineering • scaffold • stem cells

INTRODUCTION

The field of tissue engineering is progressing from a focus on structurally simple tissues or those that have significant natural regenerative capabilities to more complex tissues, coincident with the development of more advanced technologies (1, 2). With this progress, there has been a tremendous demand to produce more suitable materials and processing techniques to address the requirements (e.g., mechanical properties) of these more intricate organs and tissues (3). This demand has inspired many investigators either to modify the existing synthetic and natural polymers (e.g., the introduction of controlled degradation) (4, 5) or to generate novel synthetic polymers with diverse properties for a wide range of tissue engineering applications (6−12).

As an example, poly(glycerol sebacate) (PGS) was developed to fulfill an unmet material need for the engineering of soft tissues by introducing a polymer with elastic properties that can also degrade and support cellular adhesion and proliferation (6). Recently, the synthetic scheme of PGS was modified to incorporate reactive acrylate groups (Acr-PGS), which introduces the spatial and temporal benefits of radical cross-linking (e.g., photo-cross-linking) to overcome the limitation of the high temperature and vacuum required to cure PGS, thus extending its processing capabilities (13−15). The bulk properties of Acr-PGS networks are controlled by simple adjustments during macromer synthesis (e.g., the macromer molecular weight and percent acrylation), thus rendering the system tunable with respect to mechanics and degradation (13).

Beyond bulk polymer properties, investigators have recently begun to recognize the importance of the microenvironment's structure on controlling cellular behavior. For example, mesenchymal stem cells (MSCs), which are increasingly utilized for tissue engineering applications, respond very differently to two-dimensional versus three-dimensional environments (e.g., fibrous structures) (16−18). Within the past decade, electrospinning has become a popular technique to create fibrous scaffolds that have a size scale and architecture similar to those of the native extracellular matrix (19−22). These scaffolds may be particularly useful for fiber-aligned tissues (e.g., meniscus, myocardium) and can be aligned for anisotropic properties and cellular behavior (22, 23).

Several important processing variables (e.g., applied voltage, flow rate) need to be considered when attempting to electrospin a new polymer (24). For example, the molecular

* To whom correspondence should be addressed. E-mail: burdick2@seas.upenn.edu. Tel.: 1-215-898-8537. Fax: 1-215-573-2071.
Received for review June 10, 2009 and accepted August 30, 2009
[†] University of Pennsylvania.
[‡] Columbia University.
DOI: 10.1021/am900403k

Published on Web 09/11/2009

weight and polydispersity are related to the chain entanglement ratio, which dictates electrospun fiber formation for a particular polymer (25). For low-molecular-weight reactive polymers that do not meet this criteria, the introduction of a carrier polymer [e.g., poly(ethylene oxide), PEO] into the electrospinning solution can be used for processing. If an initiator is electrospun with a reactive polymer, the radical polymerization can be performed with the introduction of a light source after fiber formation (13, 21). Gelatin has been successfully blended with various synthetic polymers, such as PLA (poly(lactic acid)) (26) and PCL (polycaprolactone) (27, 28), to improve cellular interactions when compared to fibrous meshes of those polymers alone (26, 28–30), thus making it attractive as a possible carrier polymer to facilitate the electrospinning of Acr-PGS.

The objective of this work was to synthesize a collection of Acr-PGS macromers that cross-link into networks with a range of material properties (e.g., mechanics and degradation) and that can be electrospun into fibrous scaffolds with gelatin as a carrier polymer to facilitate cellular adhesion. This system was designed for applications that require a fibrous scaffold that is also biodegradable, supports cellular adhesion, and has tunable properties. To illustrate this, the scaffold biomechanics, degradation kinetics, and cellular interactions between the bulk polymers and electrospun scaffolds were investigated. Prior work has demonstrated that bulk polymer networks formed from these macromers elicit a nontoxic response and result in only a thin fibrous capsule after subcutaneous implantation (13). Therefore, as an initial proof of concept, the capability of utilizing Acr-PGS electrospun scaffolds for a soft tissue application was explored by implanting it as a cardiac patch in a rat model of myocardial infarction.

EXPERIMENTAL SECTION

Macromer Synthesis. All reagents were purchased from Sigma Chemical Co. (St. Louis, MO) and used as received unless noted. Acr-PGS was synthesized as previously described (13). Briefly, the PGS prepolymer was formed by the condensation reaction of equimolar amounts of glycerol (ThermoFisher Scientific, Waltham, MA) and sebacic acid. The reagents were combined at 120 °C under nitrogen for 2 h before a vacuum was applied for 72 h. The resulting branched prepolymer was directly split into three groups of equal mass. For acrylation, prepolymers were dissolved in methylene chloride (1:10, ThermoFisher Scientific) containing triethylamine (TEA; equimolar to acryloyl chloride) and 500 ppm of 4-methoxyphenol (MeHQ). Each prepolymer group (termed Low, Mid, and High) was reacted with a different molar ratio of acryloyl chloride [10, 15, and 30%, respectively, 1:10 (v/v) in methylene chloride], which was slowly dripped into the solution. These molar ratios were calculated using the estimation that two of the three hydroxy groups present in glycerol reacted with sebacic acid during the condensation reaction and are meant to provide a range of overall acrylations. An additional 500 ppm of MeHQ was added to the reaction flask, and a rotary evaporator (40 °C, 450 mbar) was used to remove methylene chloride. Ethyl acetate was added to the reaction flask, and the solution was filtered to remove the TEA salts and washed three times with 10 mM hydrochloric acid to remove any remaining salts and unreacted acrylic acid (ThermoFisher Scientific). Ethyl acetate was removed via rotovapping (40 °C, 99 mbar) to leave a viscous liquid, which was redissolved in methylene chloride and stored at 4 °C. The prepolymer molecular weights were verified using gel permeation chromatography (GPC; Waters GPC System, Milford, MA), and acrylation was assessed with ^{1}H NMR spectroscopy (Bruker Advance 360 MHz, Bruker, Billerica, MA). Macromers were mixed with 0.5 wt % (with respect to the mass of the macromer) of the photoinitiator 2,2-dimethoxy-2-acetophenone (10 wt % in methylene chloride).

Table 1. Concentration of the High Acr-PGS Macromer and Gelatin in Electrospinning Solutions

Acr-PGS/gelatin ratio (v/v)	electrospinning solution concn (wt %)		scaffold composition (wt %)	
	Acr-PGS	gelatin	Acr-PGS	gelatin
30:70	15	7	68.2	31.8
40:60	20	6	76.9	23.1
50:50	25	5	83.3	16.7

Table 2. Synthesized Acr-PGS Macromers with Constant Molecular Weight and Variable Acrylation

macromer	M_n (kDa)	M_w (kDa)	% acrylation
High	3.74	24.24	23.5
Mid	3.74	24.24	14.2
Low	3.74	24.24	1.04

Fabrication of Electrospun Acr-PGS Scaffolds. Solutions for electrospinning were prepared by dissolving the macromer/initiator in 1,1,1,3,3,3 hexafluoro-2-propanol (HFIP; 50 wt %). In order to facilitate fiber formation, the macromer/HFIP solution was combined with 10 wt % gelatin B (from bovine skin) in HFIP (dissolved in a sealed vial at 50 °C for 2 h to prevent evaporation). Various solutions containing different ratios of Acr-PGS and gelatin (Table 1) were electrospun at room temperature using a flow rate of 1.5 mL/h, a distance to the collection plate of 10 cm, and a +15 kV applied voltage. Scaffolds were cross-linked with exposure to ~10 mW/cm^2, 365 nm ultraviolet light (Blak-Ray, Ultraviolet Products, Upland, CA) in a nitrogen atmosphere. Scaffolds were gold-sputter-coated and viewed using scanning electron microscopy (SEM; JEOL 6400 or JEOL 7500 HR-SEM, Tokyo, Japan). Fiber diameters (n = 50) were quantified from the SEM images using NIH *ImageJ* software. The High macromer formulation (Table 2) was used for all initial testing.

Network Characterization. For studies performed on bulk materials, macromer/initiator solutions were poured into a 50 × 15 × 1 mm Teflon mold and placed in a vacuum oven at 60 °C overnight to remove methylene chloride. The sample was then polymerized with exposure to ~10 mW/cm^2, 365 nm ultraviolet light (Blak-Ray) for 10 min on each side. Prior work demonstrated that these conditions lead to maximum acrylate conversion (13, 21). For in vitro degradation studies, samples (10 × 2 × 1 mm) were immersed in phosphate-buffered saline (PBS) at 37 °C with frequent PBS changes. At each time point, samples (n = 3) were removed, lyophilized (Freezone 4.5, Labconco, Kansas City, MO) for 24 h, and weighed to determine the mass loss. The contact angle of 100 μL of water on the bulk polymer surfaces (n = 3) was assessed using the static sessile drop technique (CAM-Plus Micro, Tantec, Fairfield, OH). The amount of unreacted macromer (sol fraction) of the networks was determined as the mass loss following incubation of bulk polymer disks (n = 3, 4 mm diameter × 1 mm thickness) in methylene chloride for 72 h, which allowed unreacted macromer to swell free of the network.

Samples for mechanical testing (n = 4–6, 15 × 5 × 1 mm for slabs and 25 × 5 × 1 mm for scaffolds) were cut, and uniaxial tensile testing was performed on an Instron 5848 mechanical tester (Canton, MA) at a strain rate of 0.1%/s. For

fibrous scaffolds, samples (both dry and after incubation in deionized water for 1 h) were preloaded with 0.5 N at 0.5% strain for 60 s, followed by preconditioning with 10 sinusoidal cycles of 0.5% strain at 0.1 Hz prior to testing to failure. The tensile modulus of the construct was calculated from the linear region of the stress−strain curve (0−3%) and initial sample geometry.

Cytotoxicity and Cell Adhesion. To evaluate indirect cytotoxicity of the bulk Acr-PGS materials, polymer disks (4 mm diameter × 1 mm thickness) were prepared as described above. Samples were incubated in PBS overnight, sterilized with exposure to a germicidal lamp in a laminar flow hood for 30 min per side, and placed in transwell inserts above cultures of human MSCs (hMSCs, Lonza, seeded 24 h previously at 6000 cells/cm^2) maintained in standard growth media consisting of Alpha-MEM (Gibco, Invitrogen, Carlsbad, CA) supplemented with 16.7% fetal bovine serum (Gibco), 1% penicillin (Gibco), and 1% streptomycin (Gibco). Cell proliferation was measured using the AlamarBlue (AB; Invitrogen) fluorescence assay. Growth media containing 10% (v/v) AB were added to each well. After a 4 h incubation period, 100 μL aliquots (n = 3/group) of the AB-containing media were removed from each well for fluorescence measurement (530 nm excitation, 590 nm emission; Synergy HT, Biotek Winooski, VT). Blank control samples for each group (tissue culture plastic, High, Mid, and Low) in growth media without cells were also treated in order to account for any background fluorescence. Samples were then fed with fresh growth media without AB. For continual assessment, the AB assay was completed every other day on the same population of cells up to day 3 after exposure to the polymer.

For bulk cell adhesion studies, the macromer/initiator solution was dissolved in ethanol (50 wt %) and 35 μL of this solution was added into the wells of a 24-well plate. Ethanol was evaporated off overnight, and macromers were cured under a nitrogen purge and ultraviolet light (Blak-Ray) for 10 min. Films were incubated in PBS overnight and sterilized with exposure to a germicidal lamp in a laminar flow hood for 30 min, followed by incubation with growth media for 2 h prior to seeding. hMSCs were seeded onto the films at 6000 cells/cm^2, and the AB assay was used to monitor cell proliferation every other day until day 7. At the same time points, cells were rinsed three times with PBS and fixed in 4% formalin for 10 min. The cells were permeabilized with 0.25% Triton X-100 in PBS for 10 min, and nonspecific binding sites were blocked with 3% bovine serum albumin and 0.1% Tween-20 in PBS for 15 min. Actin stress fibers were stained using FITC-conjugated phalloidin (0.66 μg/mL in a blocking solution) for 40 min at 37 °C. Films were rinsed three times with PBS at each step, and images were taken on a fluorescent microscope (Axiovert, Zeiss, Berlin, Germany) with a digital camera (Axiovision, Zeiss). Images were postprocessed using NIH *ImageJ* software.

To investigate cellular interactions with the Acr-PGS/gelatin fibers, samples were prepared by electrospinning each macromer/gelatin solution onto glass coverslips (22 × 22 mm; Corning, Lowell, MA) for 40 min with the previously mentioned electrospinning parameters. To ensure that the scaffolds adhered to the glass, the coverslips were treated with poly[(3-trimethoxysilyl)propyl methacrylate] (TMSMA), as was previously described (31) prior to electrospinning. Briefly, coverslips were plasma-treated for 3 min (700 mAmp, Plasma Prep II; SPI Supplies, West Chester, PA), coated with TMSMA, baked at 100 °C for 30 min, baked at 110 °C for 10 min, washed with deionized water, and dried overnight. After electrospinning, samples were maintained under a vacuum overnight to ensure complete solvent removal, photo-cross-linked as above with ultraviolet light (Blak-Ray) in a nitrogen atmosphere, and incubated in PBS overnight. Samples were placed in nontreated wells of a 6-well plate, sterilized, seeded with hMSCs, and assessed for viability and morphology (with the addition of DAPI, 2 μg/mL) as described above. Cell proliferation was also evaluated using the AB assay, and cells were imaged as above.

In Vivo Assessment. Scaffolds from the High, Mid, and Low groups (~7.0 mm^2) were evaluated in the rat model of acute myocardial infarction for their ability to attach to the infarct bed and for their biodegradation behavior. All groups were compared at the 2-week time point (n = 3; scaffold thickness 150 μm), and the High group (n = 3; scaffold thickness 300 μm) was additionally evaluated at 4 weeks. Infarcted and untreated (scaffold-free) animals were used as controls. Rowett (rnu/rnu) athymic nude rats (body weight of 225−250 g; Harlan Sprague Dawley, Indianapolis, IN) were used in studies approved by the Columbia University Institutional Animal Care and Use Committee. Similar to the work of Fujimoto et al. (32), rats were anesthetized with inhaled isoflurane (2−3%), endotracheally intubated, and mechanically ventilated. The heart was exposed through a left thoracotomy and the pericardium incised. The left anterior descending (LAD) artery was then permanently ligated with a 7-0 prolene suture 2−3 mm below the edge of the left atrium. The scaffold (7.0 mm^2) was then sutured directly onto the epicardial surface of the infarct bed using four 7-0 prolene stay sutures in each corner of the scaffold. Scaffolds covered ~20% of the epicardium. Scaffolds were implanted 20 min postligation, and the ribs were reapproximated and the soft tissue closed in two layers. A total of 2 or 4 weeks after patch implantation, rats were sacrificed and intact hearts were collected for histology. Samples were stained using hematoxylin and eosin and the Masson trichrome stain to evaluate the extracellular matrix.

Statistical Analysis. All data are presented as mean ± standard deviation. Comparisons using a Student's t test assuming unequal variances were used for data in which the variances between groups were not equal; otherwise, a single factor ANOVA with Tukey's post hoc test was used to determine the statistical significance among groups with $p < 0.05$.

RESULTS AND DISCUSSION

As the field of regenerative medicine advances, there is a need to develop alternative materials and scaffold processing techniques to closely mimic the properties of the surrounding native tissue. Elastomers, such as PGS, are attractive for tissue engineering applications because of their ability to undergo large, reversible deformations with complete recovery (25) and possibly attenuate the compliance mismatch problem that often exists with synthetic polymeric implants in various dynamic environments that exist in the body, such as in the heart (6). To further exploit the potential of the synthetic elastomer PGS, acrylate functional groups (Acr-PGS) have been introduced, such that cross-linking can take place under relatively mild conditions with the use of a photoinitiator and light (13, 15). The specific focus of our study was to establish a process for the fabrication of fibrous elastomer scaffolds with a range of mechanical and degradation properties for soft tissue engineering and to test in a preliminary way the utility of these scaffolds in a heart infarction model. We propose that the wide range of biomechanical properties (tensile modulus ranging from ~60 kPa to 1 MPa) and degradation rates (~45−70% mass loss by 12 weeks) of these scaffolds enables their custom design for a variety of tissue engineering applications.

Macromer Synthesis and Scaffold Fabrication. Acr-PGS was synthesized using a condensation reaction of glycerol with sebacic acid that is further reacted with acryloyl chloride (Figure 1). The use of trifunctional glycerol in the

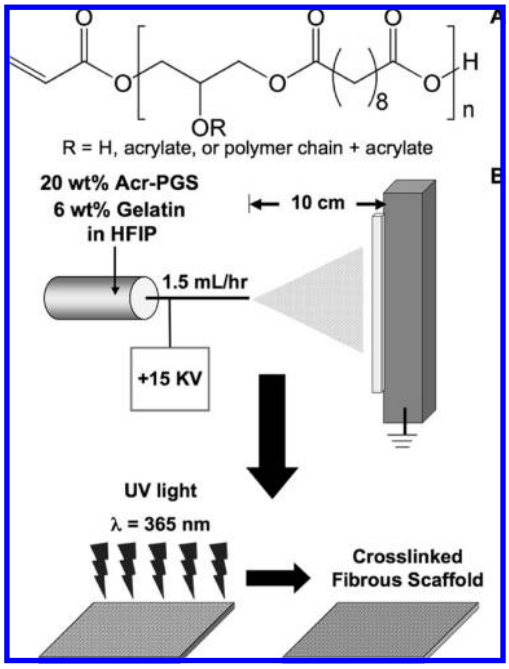

FIGURE 1. Macromer synthesis and scaffold preparation. Structure of the reactive Acr-PGS macromer (A). Schematic of the electrospinning process (B). A solution of Acr-PGS macromer, gelatin, and the photoinitiator in HFIP is electrospun to form a fibrous mat of Acr-PGS and gelatin. The scaffold is subsequently exposed to ultraviolet light to form cross-linked fibrous scaffolds.

condensation reaction introduces the possibility of branching, and the resulting fraction of hydroxyl groups converted during acrylation leads to a relatively complex macromer structure. A representative ^{1}H NMR spectral example with peak assignments can be found in our previously reported work (13). The bulk network properties (i.e., mechanics and degradation) of Acr-PGS networks can be tuned for a particular application by altering both the prepolymer molecular weight and the amount of acrylate functional groups introduced into the macromer system (13, 15). In this work, a small collection of Acr-PGS macromers was synthesized with the same molecular weight but with variable acrylation. On the basis of previous work, a wider range of bulk network properties was obtained using a prepolymer molecular weight of approximately 20–25 kDa (13); therefore, a batch of PGS prepolymer was synthesized with a similar prepolymer weight-average molecular weight of 24.24 kDa, as verified by GPC (Table 2). The prepolymer was then divided and acrylated to various extents (defined as Low, Mid, and High) as determined by ^{1}H NMR (Table 2).

In order to successfully electrospin Acr-PGS scaffolds, a carrier polymer was needed to facilitate fiber formation because of the relatively low molecular weight of Acr-PGS compared to that of commonly electrospun polymers (e.g., PCL, 80 kDa) (19, 23). For example, PEO has been successfully utilized as a carrier polymer to electrospin poly(β-amino ester)s of relatively low molecular weight (~4 kDa) (21). Once the reactive macromer is cross-linked with ultraviolet light, a semi-interpenetrating network is formed. However, if PEO is used, there is the potential that it will not completely swell from the fibers and will block protein adsorption and, as a result, limit cell adhesion (21). With this concern in

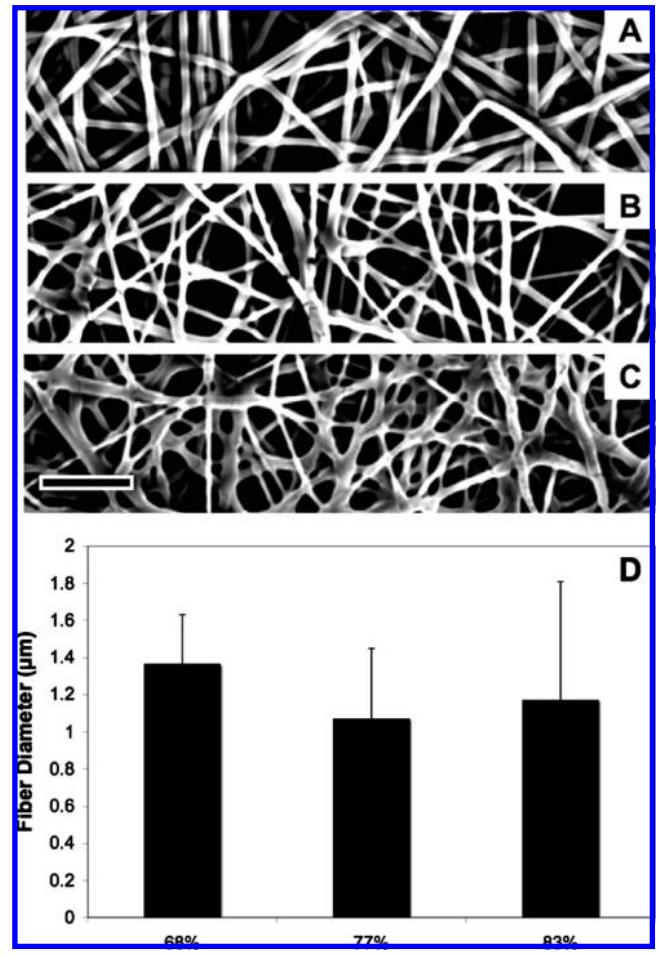

FIGURE 2. Influence of the Acr-PGS/gelatin ratio on fiber formation. SEM images of scaffolds with Acr-PGS concentrations of 68.2% (A), 76.9% (B), and 83.3% (C) by mass in the resulting mat. Fiber diameter as a function of the Acr-PGS concentration (D). The High macromer was used for this initial study. Scale bar = 10 μm.

mind, gelatin was investigated as an alternative carrier polymer because of its ability to improve cell adhesion in electrospun scaffolds when blended with other synthetic polymers (26–30).

It is known that the ratio of reactive macromer to carrier polymer in the blend is important in determining the resulting fiber morphology (13, 21). Therefore, the macromer (High Acr-PGS) and gelatin were combined in various ratios (Table 1) and electrospun, and the resulting fiber morphologies were investigated using SEM after photo-cross-linking (Figure 2). We have previously demonstrated that these macromers reach high double-bond conversions during photopolymerization, both in the bulk and as scaffolds composed of similar reactive polymers at a depth of 1 mm (13, 21). Fibers were formed with all ratios of Acr-PGS to gelatin with diameters in the range of 1.0–1.4 μm. There were no statistical differences in the fiber diameters as a function of the Acr-PGS concentration. However, as the amount of Acr-PGS in the blend was increased, there was an increase in the webbing between the fibers and a decrease in the fiber uniformity (Figure 2). The mass ratio of 77% Acr-PGS to 23% gelatin in the resulting fibrous mesh was selected as the optimal ratio for further experiments in

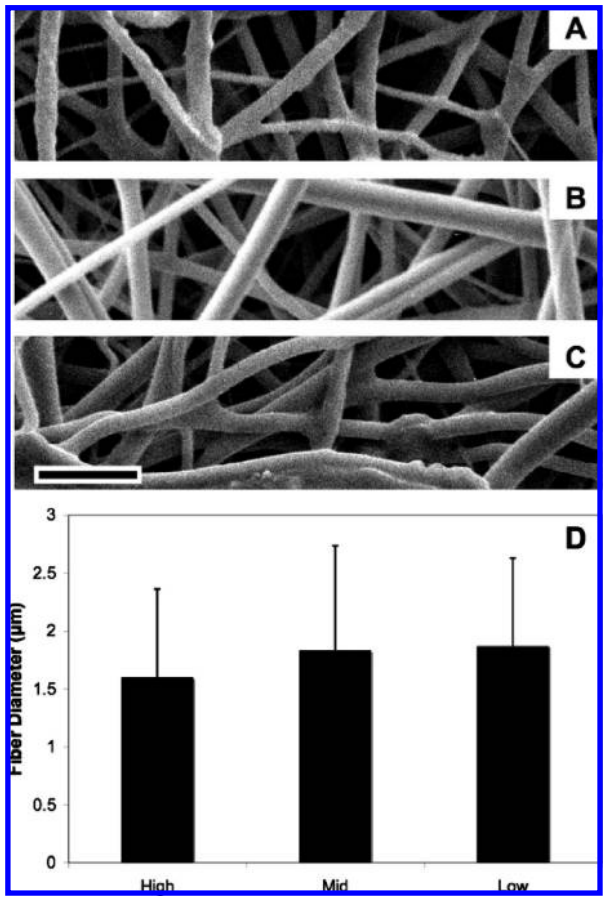

FIGURE 3. Influence of Acr-PGS acrylation on fiber formation. SEM images of scaffolds fabricated from the three different Acr-PGS macromers, High (A), Mid (B), and Low (C), using gelatin as a carrier polymer and a final mass ratio of 77 wt % Acr-PGS to 23 wt % gelatin. Fiber diameter as a function of the degree of acrylation (D). Scale bar = 10 μm.

order to maintain Acr-PGS as the majority of the scaffold for control over the mechanics and degradation of the scaffolds while providing relatively uniform fibers. In order to ensure that any differences in the mechanics, degradation, or cellular responses are due to the Acr-PGS macromer used for scaffold fabrication, the two additional Acr-PGS macromers (Mid and Low) were electrospun with gelatin at this same concentration and evaluated using SEM (Figure 3). Fibrous scaffolds with relatively uniform morphology were formed from all macromers without statistical differences in the fiber diameter between scaffolds prepared from different macromers.

Characterization of Network Properties. The bulk polymer network properties for contact angle, sol fraction, and mechanics and degradation were characterized. The contact angle of the bulk polymers was calculated using the sessile drop method. There is a decrease in both the contact angle and sol fraction as the percent acrylation increases (Table 3). The probability of cross-link formation between the macromers decreases as the number of acrylate groups is reduced, thereby increasing the number of soluble oligomers formed.

The mechanical properties of bulk Acr-PGS and Acr-PGS/gelatin fibrous scaffolds both dry and hydrated were evaluated using uniaxial tensile testing (Figure 4). As expected, a range of magnitudes in both the Young's modulus and extension at break were observed as the acrylation concentration varied. For bulk polymer networks, the Young's moduli (from ~31 kPa to 6.6 MPa) increased and the extension at break (from ~110 to 9%) decreased with

Table 3. Properties of the Bulk Polymer Networks Formed from the Three Different Macromers

bulk polymer network	contact angle (deg)	sol fraction (%)
High	55.69 ± 4.74	13.34 ± 0.90
Mid	70.36 ± 3.93	32.00 ± 2.78
Low	85.62 ± 13.74	51.91 ± 2.81

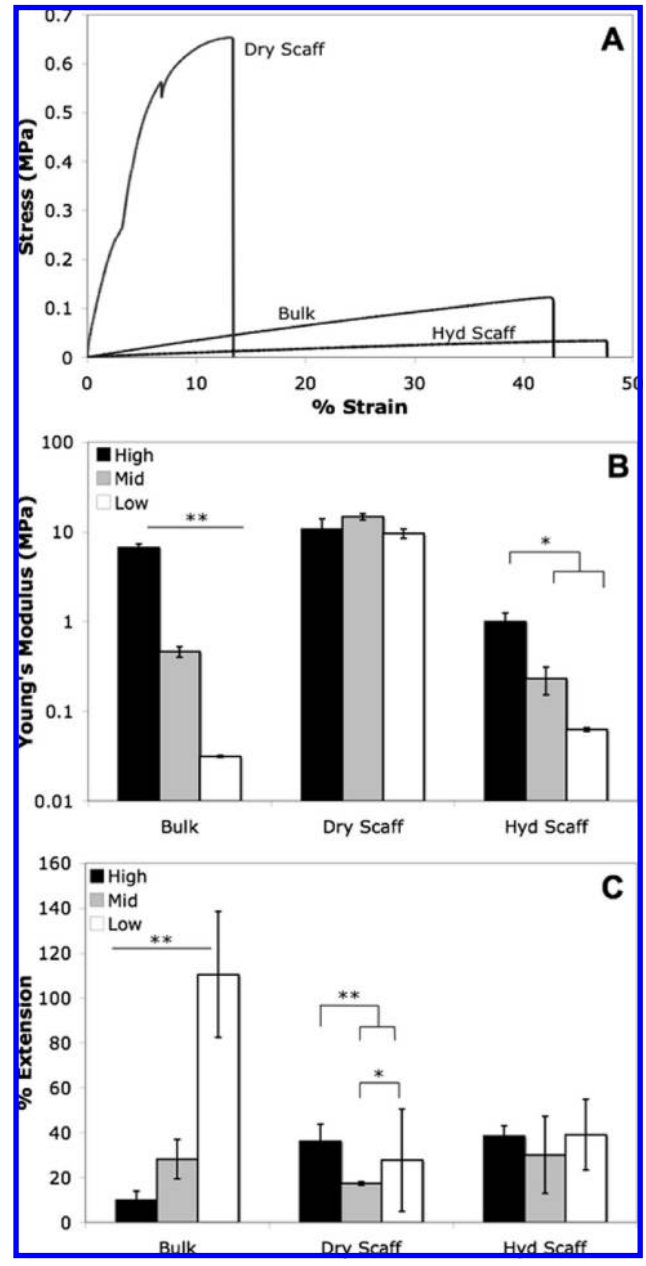

FIGURE 4. Representative stress versus strain curves for groups prepared from the Mid macromer (A). Tensile properties of bulk polymers, dry scaffolds, and hydrated scaffolds for the High (black), Mid (grey), and Low (white) macromers for Young's modulus (B) and percent extension (C): (*) $p < 0.05$; (**) $p < 0.01$.

increasing amounts of acrylation in the Acr-PGS backbone (Figure 4). There were statistically significant differences in both of these properties between all acrylation groups. It is important to note that the samples often broke at the clamps and thus may be reported as lower than the actual values with respect to the extension at break.

The fibrous scaffolds were tested both in the dry state and following incubation in water for 1 h in order to investigate the mechanical properties under more physiological conditions, such as those found in vivo. In the dry state, there is relatively little variation and no statistical difference in the modulus of the scaffold between acrylation groups. This could be due to the gelatin, which has been reported to have a modulus of ~500 MPa for similar electrospun scaffolds tested in the dry state under tension (30), dominating the mechanics in the dry state. This is evident by a substantial increase in the modulus to ~10 MPa in the fibrous state compared to that of the slab form in samples prepared from the various macromers (Figure 4). However, when the samples are hydrated, the degree of acrylation of Acr-PGS appears to have more influence over the mechanics of the scaffolds, with similar trends in the moduli between the groups, as was observed for the bulk samples (Figure 4). Because of premature failure at the grips, substantial changes in the extension with the extent of acrylation are not reflected in the collected data. The tested hydrated scaffolds lost ~9% of their mass (across all groups, data not shown) within the hour of hydration, presumably because of gelatin and small amounts of unreacted macromer being leached from the scaffolds. The variability between the dry and hydrated samples is most likely due to water absorption by the remaining gelatin component, thus forming a resilient, hydrated composite. These values are lower than those reported in the literature for pure gelatin scaffolds (29, 30) because the scaffold is composed of only ~23% gelatin. Moreover, the formation of scaffolds consisting of gelatin alone cannot be directly compared to the blended scaffolds because of the cross-linking (i.e., with glutaraldehyde) necessary for stabilization. Here, a stable interpenetrating blended network that does not require secondary chemical cross-linking of the gelatin is obtained. This is advantageous because further chemical cross-linking of the gelatin may result in an increase in the rigidity of the scaffolds and a decrease in the effectiveness of the gelatin with respect to cell adhesion (29).

The in vitro degradation of the Acr-PGS bulk polymers and scaffolds was monitored over an 18-week period. Within each formulation (bulk versus fibrous scaffold), the mass loss correlated with acrylation, with the Low group losing mass faster than the Mid group, which was faster than the High group. The mass loss in these systems is a combination of the gelatin release, sol fraction, and hydrolysis of the cross-linked Acr-PGS into its naturally derived monomers sebacic acid and glycerol and a relatively low concentration of poly(acrylic acid) kinetic chains. Because HFIP is the only solvent in which both the macromers and gelatin are soluble, ^{1}H NMR cannot be utilized to determine the relative ratios

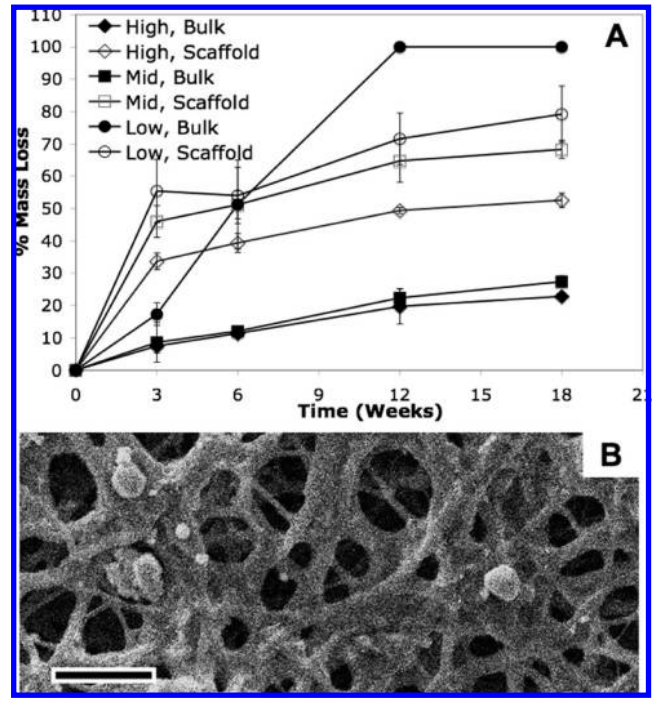

FIGURE 5. In vitro mass loss for High (diamonds), Mid (squares), and Low (circles) groups processed as slabs (filled symbols) and fibrous scaffolds (open symbols) with time (A). SEM image of the Mid scaffold at 6 weeks of degradation in PBS (B). Scale bar = 10 μm.

of components released. It is not surprising that the samples with fewer acrylates degraded more quickly because there are fewer cross-links to degrade prior to mass release and there is a higher sol fraction present. Additionally, scaffolds degraded at a faster rate than their respective bulk macromer counterpart with the exception of the bulk Low material, which degraded completely within 12 weeks (Figure 5A). This inconsistency could potentially be due to enhanced polymer entanglement in the fiber form compared to the bulk samples. An initial increase in the mass loss of the scaffolds is observed up to 3 weeks, which is most likely due to some loss of the gelatin carrier polymer in the interpenetrating network to the aqueous medium. Therefore, it is impossible to directly compare the degradation rates of the scaffolds and bulk polymers, which do not incorporate gelatin. The scaffolds maintained their fibrous nature with degradation, as observed in the SEM image of the Mid fibrous scaffold after 6 weeks (Figure 5B). Note that residual salts from the PBS are also observed.

Cytotoxicity and Cell Adhesion. In order to evaluate the cytotoxicity of the Acr-PGS macromers, hMSCs were cultured in the presence of the bulk Acr-PGS materials, without having direct contact with the polymer. This assay provides information on the potential toxicity of leachable components and degradation products from the samples. The wells were confluent at 3 days, and no statistical differences in fluorescence (i.e., metabolic activity) between the cells cultured with or without polymer present were observed (results not shown). Thus, changes in the direct cellular interactions may be attributed to nonoptimized integrin binding rather than toxic elements from the systems.

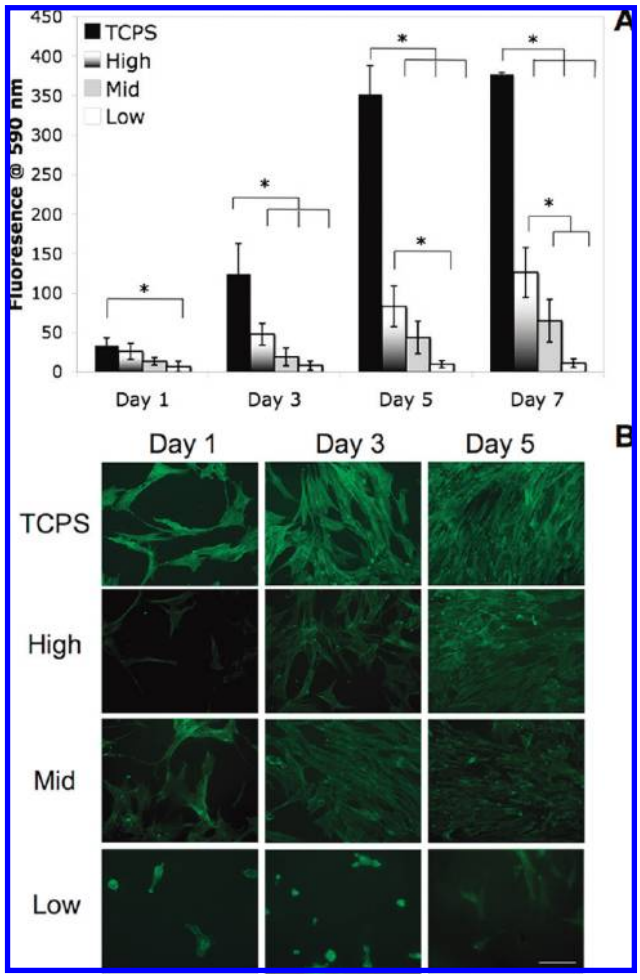

FIGURE 6. Bulk cell interactions between hMSCs and Acr-PGS networks. hMSC metabolic activity/proliferation, as measured by fluorescence, over 7 days using the AB assay (A). Fluorescent images of hMSC morphology (actin fiber staining) when cultured on thin films of the Acr-PGS macromers (B): (*) $p < 0.05$. Scale bar = 100 μm.

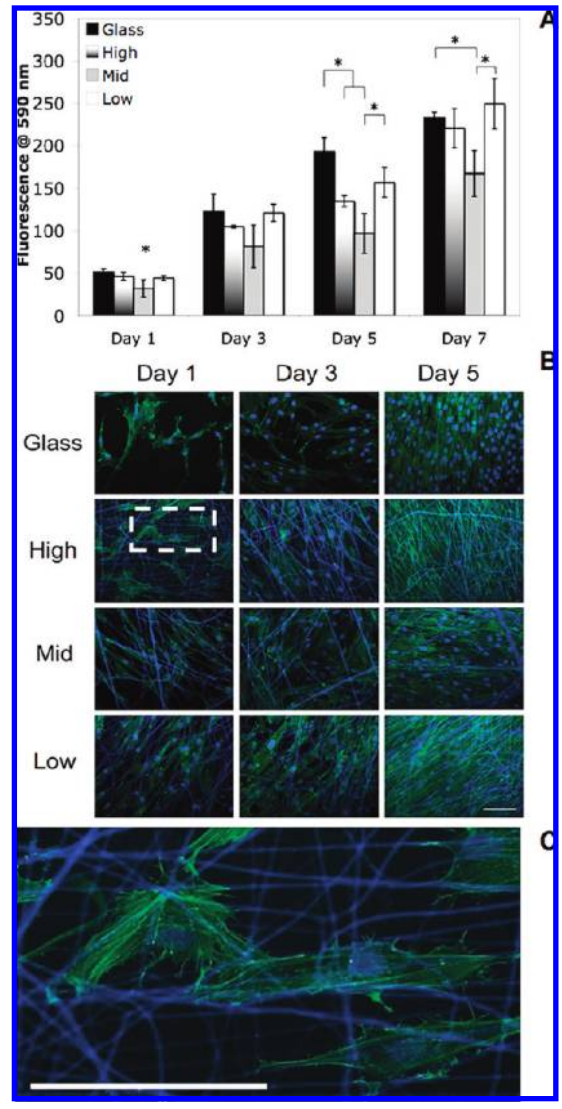

FIGURE 7. hMSC interactions with scaffolds prepared with the different Acr-PGS macromers. hMSC metabolic activity/proliferation, measured by fluorescence, on the different scaffolds over 7 days, using the AB assay (A). Fluorescent images of actin stress fibers (green) and electrospun fibers (blue) depicting the morphology of hMSCs cultured on the different scaffolds (B). Magnified image of the inset at day 1 depicting the direct cellular interactions with hMSCs and electrospun fibers (C): (*) $p < 0.05$. Scale bar = 100 μm.

When hMSCs were seeded directly on films of the polymers, the metabolic activity of the cells cultured on the polymers was significantly lower than that of cells cultured on tissue culture plastic (Figure 6A). However, as is evident from actin staining and an increase in fluorescence with culture, cells appear to adhere, spread, and proliferate on films prepared from the High and Mid Acr-PGS macromers (Figure 6B). Cellular viability and adhesion are significantly reduced on the Low polymer, where the majority of cells were rounded (Figure 6A,B). There are several reasons that cellular interactions may not be optimized for interacting with the Acr-PGS networks, including nonoptimal protein adsorption, mechanics, and the tackiness of the material. In previous studies, greater cell attachment was observed on surfaces with intermediate contact angles versus surfaces with higher or lower contact angles (33−35). For example, polystyrene and poly(ethylene terephthalate) are moderately hydrophobic polymers (contact angles ~60−70°) that support greater cell attachment compared to highly hydrophilic polymers, such as cellulose (contact angle ~18°) or tetrafluoroethylene hexafluoropropylene (contact angle ~102°) (35). The variability in the contact angles in our study may contribute to differences in cellular responses; however, the lack of toxicity in the noncontact study indicates that it is not likely due to the release of any cytotoxic components. Thus, the significant difference in the metabolic activity between tissue culture plastic and the High and Mid films is most likely due to poor cell attachment initially (day 1, Figure 6A) resulting from suboptimal protein absorption.

However, the cellular viability and morphology was very different on thin scaffolds that were electrospun with gelatin present compared to thin polymer films. Specifically, cell attachment and proliferation were similar for electrospun fiber scaffolds and glass coverslips (Figure 7A), with confluent monolayers found within 7 days postseeding for all formulations. Cells appear to adhere and spread over the fibers (Figure 7B), which are readily visualized because Acr-PGS interacts with the DAPI nuclear stain. Cells were ex-

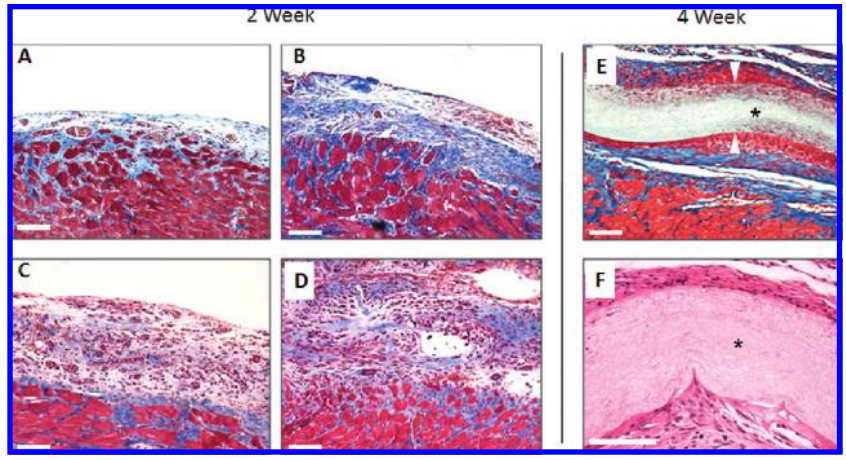

FIGURE 8. In vivo tissue response to Acr-PGS scaffolds. The scaffolds were implanted epicardially post-LAD-ligation for 2 or 4 weeks. Trichrome staining of the control (A) and Low (B), Mid (C), and High (D) scaffolds at 2 weeks. A thicker High scaffold was implanted and observed at 4 weeks using trichrome staining (E) and H&E (F). The asterisk marks the center of the scaffold, while the arrows delineate the edges. Scale bar = 50 μm.

tending pseudopodia and interacting with individual fibers (Figure 7C) for scaffolds formed from all three macromers. This is in contrast to studies in which PEO was used as a carrier polymer with Acr-PGS and cells remained spherical and not spread along the fibers (data not shown); thus, cell adhesion and spreading can be attributed to the gelatin. The increase in cell attachment and proliferation compared to that of the bulk polymers may result from differences in the surface topography or the presence of gelatin as the carrier polymer in this system, therefore eliminating the reliance on protein adsorption from serum to facilitate cell adhesion.

In Vivo Assessment. The initial tissue response and capacity of the scaffolds to function within a therapeutically relevant scenario were evaluated using a rat model of acute myocardial infarction. This study was designed to investigate the feasibility of applying these scaffolds to the infarct bed and to obtain preliminary insights into the effects of scaffold properties (stiffness and degradation) on tissue outcomes in this experimental model. Scaffolds from the three different Acr-PGS macromers (High, Med, and Low) were assessed at a 2-week time point; scaffolds from the High group were additionally evaluated at the 4-week time point. The scaffold-free control shows some collagen deposition consistent with normal post-MI fibrosis (Figure 8A). Notably, the scaffolds from all three groups were entirely degraded over the 2-week period of implantation (Figure 8B–D). The rapid degradation compared to that of the in vitro samples may be due to the inflammation and cellular infiltration in the postinfarct environment, which may have contributed to the increased hydrolysis of the scaffolds. This effect was clearly seen because the scaffolds were very thin (~150 μm compared to 1 mm for in vitro studies).

Interestingly, there was a correlation between the tissue response and the amount of acrylation. The Low acrylation macromer samples showed increased collagen deposition compared to that of the scaffold-free control (Figure 8A). However, there were only a few inflammatory cells present after 2 weeks. For the Mid macromer group, inflammatory cells were still present, despite the scaffold being mostly degraded. Numerous arterioles were consistent with the early resolution stages of inflammation (Figure 8B). A greater amount of inflammation in the infarct area with many granulocytes visible was observed where the High macromer group scaffolds were implanted (Figure 8D). In summary, a more resolved inflammatory response with evidence of collagen deposition was observed for Low samples, whereas the Mid and High samples demonstrated an unresolved host response because of the high levels of inflammation. Notably, the rapid degradation that was observed in this environment leads to rapid release of degradation products locally, which explains the tissue response. Our further studies will determine the relative contributions of the rate of degradation and local mechanics to these differences in scaffold behavior.

After complete degradation of the 150-μm-thick scaffolds was observed at 2 weeks, the study was repeated using 300 μm scaffolds of the High macromer to study a longer term response (4 weeks in vivo) of the host to the material. The scaffolds were still present at 4 weeks, and cellular infiltration was observed only in the outer portion of the scaffold (Figure 8E), which may lead to higher local concentrations of enzymes and, therefore, degradation. The center of the scaffold is marked by an asterisk, and the arrows mark the edges (Figure 8E,F). The scaffold was not fully degraded and was covered with the host's foreign body capsule. Greater detail of the capsule using H&E staining shows a minimal presence of granulocytes and a resolved inflammatory response with significant fibrosis at the 4-week time point (Figure 8F). This pilot study demonstrates the feasibility of suturing electrospun scaffolds composed of Acr-PGS and gelatin onto the epicardial surface of the heart. Moreover, it demonstrates that the host response to the implanted material, in the setting of acute cardiac infarction, markedly depends on the scaffold thickness and degree of acrylation. Future work will involve evaluation of the potential functional improvement (i.e., left vetricle size, hemodynamic data, etc.) of animals with implanted scaffolds.

CONCLUSIONS

In this study, a small collection of biodegradable Acr-PGS macromers that could be cross-linked into networks of varying bulk properties (i.e., mechanics and degradation) was successfully synthesized and characterized. These macromers were combined with gelatin in order to fabricate electrospun scaffolds. Similar trends were observed for the bulk polymers and scaffolds, in terms of the dependence of their mechanical properties on the degree of acrylation. The rate of mass loss also correlated with the extent of acrylation, such that the more acrylated materials degraded more slowly. Cells attached and remained viable on bulk thin films of the different macromers; however, potentially suboptimal protein adsorption decreased their adhesion and metabolism relative to controls on tissue culture plastic. In contrast, cell adhesion and proliferation on electrospun scaffolds was indistinguishable from controls, possibly because of the presence of the gelatin, which decreased the dependence on adsorbed protein from serum and facilitated cell adhesion on the scaffolds. Finally, the scaffolds were implanted into a rat model of acute myocardial infarction to investigate the functional tissue response and possible use of the scaffolds for cardiac patch applications. The scaffolds were capable of being sutured onto the epicardial surface of the heart. Thin ($\sim$150 μm) samples degraded entirely in 2 weeks, and an increase in the inflammatory response was observed with increasing amounts of macromer acrylation. Thicker ($\sim$300 μm) samples were collected at 4 weeks post-implantation, and a foreign body capsule was observed, including some cellular infiltration into the scaffolds. Future work will involve further functional assessments of the implanted scaffolds and optimization of the properties for a specific application.

Acknowledgment. We are grateful for support from the American Chemical Society Petroleum Research Fund (to J.A.B.), the National Institutes of Health (Grants R01 HL076485 and P41-EB002520 to G.V.-N.), an Ashton Foundation Fellowship (J.L.I.), and the American Heart Association Predoctoral Fellowship Program (J.L.I.).

REFERENCES AND NOTES

(1) Lavik, E.; Langer, R. *Appl. Microbiol. Biotechnol.* **2004**, *65*, 1–8.
(2) Nerem, R. M. *Tissue Eng.* **2006**, *12*, 1143–1150.
(3) Levental, I.; Georges, P. C.; Janmey, P. A. *Soft Matter* **2007**, *3*, 299–306.
(4) Sahoo, S.; Chung, C.; Khetan, S.; Burdick, J. A. *Biomacromolecules* **2008**, *9*, 1088–1092.
(5) Sawhney, A. S.; Pathak, C. P.; Hubbell, J. A. *Macromolecules* **1993**, *26*, 581–587.
(6) Wang, Y. D.; Ameer, G. A.; Sheppard, B. J.; Langer, R. *Nat. Biotechnol.* **2002**, *20*, 602–606.
(7) Burdick, J. A.; Chung, C.; Jia, X. Q.; Randolph, M. A.; Langer, R. *Biomacromolecules* **2005**, *6*, 386–391.
(8) Bettinger, C. J.; Bruggeman, J. P.; Borenstein, J. T.; Langer, R. S. *Biomaterials* **2008**, *29*, 2315–2325.
(9) Guan, J. J.; Sacks, M. S.; Beckman, E. J.; Wagner, W. R. *J. Biomed. Mater. Res., Part A* **2002**, *61*, 493–503.
(10) Yang, J.; Webb, A. R.; Ameer, G. A. *Adv. Mater.* **2004**, *16*, 511–516.
(11) Webb, A. R.; Yang, J.; Ameer, G. A. *Expert Opin. Biol. Ther.* **2004**, *4*, 801–812.
(12) Anderson, D. G.; Tweedie, C. A.; Hossain, N.; Navarro, S. M.; Brey, D. M.; Van Vliet, K. J.; Langer, R.; Burdick, J. A. *Adv. Mater.* **2006**, *18*, 2614–2618.
(13) Ifkovits, J. L.; Padera, R. F.; Burdick, J. A. *Biomed. Mater.* **2008**, *3*, 034104.
(14) Ifkovits, J. L.; Burdick, J. A. *Tissue Eng.* **2007**, *13*, 2369–2385.
(15) Nijst, C. L. E.; Bruggeman, J. P.; Karp, J. M.; Ferreira, L.; Zumbuehl, A.; Bettinger, C. J.; Langer, R. *Biomacromolecules* **2007**, *8*, 3067–3073.
(16) Burdick, J. A.; Vunjak-Novakovic, G. *Tissue Eng., Part A* **2008**.
(17) Park, H.; Cannizzaro, C.; Vunjak-Novakovic, G.; Langer, R.; Vacanti, C. A.; Farokhzad, O. C. *Tissue Eng.* **2007**, *13*, 1867–1877.
(18) Godier, A. F.; Marolt, D.; Gerecht, S.; Tajnsek, U.; Martens, T. P.; Vunjak-Novakovic, G. *Birth Defects Res., Part C* **2008**, *84*, 335–347.
(19) Baker, B. M.; Gee, A. O.; Metter, R. B.; Nathan, A. S.; Marklein, R. A.; Burdick, J. A.; Mauck, R. L. *Biomaterials* **2008**, *29*, 2348–2358.
(20) Murugan, R.; Ramakrishna, S. *Tissue Eng.* **2006**, *12*, 435–447.
(21) Tan, A. R.; Ifkovits, J. L.; Baker, B. M.; Brey, D. M.; Mauck, R. L.; Burdick, J. A. *J. Biol. Mater. Res., Part A* **2008**, *87*, 1034–1043.
(22) Mauck, R. L.; Baker, B. M.; Nerurkar, N. L.; Burdick, J. A.; Li, W. J.; Tuan, R. S.; Elliott, D. M. *Tissue Eng., Part B* **2009**, *15*, 171—193.
(23) Baker, B. M.; Mauck, R. L. *Biomaterials* **2007**, *28*, 1967–1977.
(24) Shin, Y. M.; Hohman, M. M.; Brenner, M. P.; Rutledge, G. C. *Polymer* **2001**, *42*, 9955–9967.
(25) Shenoy, S. L.; Bates, W. D.; Frisch, H. L.; Wnek, G. E. *Polymer* **2005**, *46*, 3372–3384.
(26) Kim, H. W.; Yu, H. S.; Lee, H. H. *J. Biomed. Mater. Res., Part A* **2008**, *87A*, 25–32.
(27) Chong, E. J.; Phan, T. T.; Lim, I. J.; Zhang, Y. Z.; Bay, B. H.; Ramakrishna, S.; Lim, C. T. *Acta Biomater.* **2007**, *3*, 321–330.
(28) Ghasemi-Mobarakeh, L.; Prabhakaran, M. P.; Morshed, M.; Nasr-Esfahani, M. H.; Ramakrishna, S. *Biomaterials* **2008**, *29*, 4532–4539.
(29) Li, M. Y.; Mondrinos, M. J.; Chen, X. S.; Lelkes, P. I. *Tissue Eng.* **2006**, *12*, 989–989.
(30) Li, M. Y.; Guo, Y.; Wei, Y.; MacDiarmid, A. G.; Lelkes, P. I. *Biomaterials* **2006**, *27*, 2705–2715.
(31) Khademhosseini, A.; Eng, G.; Yeh, J.; Fukuda, J.; Blumling, J., III; Langer, R.; Burdick, J. A. *J. Biomed. Mater. Res., Part A* **2006**, *79*, 522–532.
(32) Fujimoto, K. L.; Tobita, K.; Merryman, W. D.; Guan, J.; Momoi, N.; Stolz, D. B.; Sacks, M. S.; Keller, B. B.; Wagner, W. R. *J. Am. College Cardiol.* **2007**, *49*, 2292–2300.
(33) Altankov, G.; Grinnell, F.; Groth, T. *J. Biomed. Mater. Res., Part A* **1996**, *30*, 385–391.
(34) Nuttelman, C. R.; Mortisen, D. J.; Henry, S. M.; Anseth, K. S. *J. Biomed. Mater. Res., Part A* **2001**, *57*, 217–223.
(35) Tamada, Y.; Ikada, Y. *J. Colloid Interface Sci.* **1993**, *155*, 334–339.

AM900403K